Numerical investigation of unsteady laminar methane/LOx flamelet at supercritical pressures

P.E. Lapenna*, P.P. Ciottoli, F. Creta, M. Valorani

Dept. of Mechanical and Aerospace Engineering,
University of Rome "La Sapienza",
Rome, Italy

Abstract

High-pressure combustion devices, such as liquid rocket engines, are usually characterized by transcritical and supercritical operating conditions. Propellants injected in the combustion chamber experience extremely high density gradients and real fluid effects. In the present study, real fluid effects on flame structure are investigated in the framework of unsteady laminar flamelet equations, a well established representation and diagnostic tool for non premixed combustion transient phenomena. Real fluid thermodynamic properties are taken into account by means of a computationally efficient cubic equation of state written in a general and comprehensive three-parameter fashion. High-pressure conditions for unsteady flame structure calculations and analysis are chosen as a representative range of a methane/liquid-oxygen rocket engine operating conditions. Particular focus is posed on the constant pressure specific heat behavior at low temperature, which influences the time evolution of the flame structure. Moreover time accurate integration of flamelet equations represent the very first building block of a conditional moment closure for supercritical turbulent combustion.

1. Introduction

High performance liquid rocket engines (LRE) widely utilize liquid hydrogen (LH2) together with liquid oxygen (LOx) as propellants, because of high specific impulse and non-toxic combustion. However liquid hydrogen has elevated operational costs and a relatively small volumetric specific impulse due to the low density even if stored at extremely high pressure [1]. These drawbacks have recently shifted considerable interest on the combustion of LOx and methane, the lightest and non-toxic hydrocarbon, as the propellants for future development of high-performance reusable LRE for both boosters and upper-stages engines [2]. Methane exhibit some advantages over large hydrocarbons such as kerosene, including a higher specific impulse, better cooling capabilities [3], and lower coking and sooting properties. In-depth and complete understanding of the complex phenomenology taking place at typical LRE thrust chamber operating conditions, is still to be fully achieved.

Operating conditions of LRE are mainly determined by chamber pressure p_C and injection temperature of the fuel T_f and the oxidizer T_{ox}, and they are usually classified with respect to the critical properties of the propellants. In most of the practical cases methane is injected in supercritical conditions ($T > T_{cr} = 190.8K$, $p > p_{cr} = 4.599MPa$) while liquid oxygen (LOx) is injected in a transcritical state ($T < T_{cr} = 154.6K$, $p > p_{cr} = 5.043MPa$). The injection temperature of LOx can be significantly lower than the critical temperature of oxygen, typically between $80K$ and $120K$ enhancing real fluid effects on both the mixing and combustion processes.

Recent numerical studies [4, 5, 6, 7, 8] on supercritical and transcritical combustion at high-pressures, starting from experimental evidence [9, 10, 11, 12, 13], are conceptually based on a single-phase mixture model of general fluids that accounts for thermodynamic non-ideality and anomalous transport properties. Thus, a general fluid is modeled as a "dense" gas with liquid like density and gas like diffusivities that does not experience any droplet formation (vanishing surface tension). A unified treatment of fundamental multispecies thermodynamics

*Corresponding author
Email address: pasquale.lapenna@uniroma1.it (P.E. Lapenna*)

is therefore mandatory [14], as well as detailed high pressure chemical kinetic mechanisms [15], in order to describe the complex phenomenology occurring in LRE combustion chambers. In this work real fluid thermodynamic properties are taken into account by means of a computationally efficient cubic equation of state written in a general three-parameter fashion [16], while most of the numerical studies on supercritical combustion so far relied on two-parameter cubic equation of the state, such as Peng-Robinson or Soave- Redlich-Kwong. This general form of cubic EoS has been used for the first time for modelling kerosene combustion [17], due to better handling of mixtures with quite different critical compressibility factor.
Recently in order to investigate on supercritical combustion characteristics, the common counterflow diffusion flames configuration has been rigorously researched both experimentally and numerically. Many fundamental characteristics have been extensively analyzed, such as the transcritical mass transfer caused by the sharp density gradient in the near critical region [18], the effects of pressure [19, 20], the flow strain rate and inlet temperature on flame structures [21], and finally heat release rate profiles and extinction limits [22, 23]. Most of the existing studies of high-pressure counterflow diffusion flames have focused on the oxygen/hydrogen system, while the pure oxygen/methane mixture is less investigated in transcritical and supercritical conditions [24]. However, these analysis are limited to steady-state flame structure, while the direct solution of the unsteady flamelet equations is more suitable for transient flame structure analysis. This feature is especially convenient when the goal is to simulate autoignition, subsequent flame propagation [20], and slow processes including radiative cooling and soot formation [21].
In the present study the unsteady features of the methane and cryogenic liquid oxygen flame structure at supercritical pressures are analyzed by means of a general fluid formulation for the unsteady laminar flamelet equation. Analysis on both forced and autoignition have been carried out so as to investigate on the transient flame structure and constant pressure specific heat behavior at low temperature, characterized by abrupt variations across the pseudocritical line, which strongly influences the time evolution of the flamelet solution.

2. Theoretical formulation

Under supercritical and transcritical conditions the mean free path becomes small enough to allow for molecular interactions to become important. This leads to significant deviations from the ideal gas assumption, which entirely neglects intermolecular interaction potential. For this reason, proper real gas relations for thermodynamic and transport properties as well as for the chemical kinetics need to be taken into account.

2.1. Real Gas Equation of state

A computationally efficient real gas equation of state (EoS) is here used, in order to avoid complex nonlinear formulations, even if several more accurate EoS exist such as the Benedict-Webb-Rubin (BWR) model. The widely used cubic form of the real gas EoS, usually written in a two-parameter form, can be recast in a convenient general three-parameter fashion RK-PR (Redlich Kwong - Peng Robinson) [16]:

$$p = \frac{\rho R_u T}{W - b\rho} - \frac{a\alpha(T)\,\rho^2}{(W + \delta_1 b\rho)\,(W + \delta_2 b\rho)} \qquad (1)$$

where p, ρ, T are fluid pressure, density and temperature, W is the molecular weight, R_u the universal gas constant and $\alpha(T)$ is a temperature correction factor. The three parameters characterizing the EoS are a, b and δ_1, whereas $\delta_2 = (1 - \delta_1)/(1 + \delta_1)$). The choice of parameters in Eq. (1) determines the particular cubic EoS.

The classical Peng-Robinson form is recovered for $\delta_1 = 1 + \sqrt{2}$ while the Soave-Redlich-Kwong form for $\delta_1 = 1$. A complete three parameter EoS, such as the RK-PR, is obtained for $\delta_1 = \delta_1(Z_c)$, where Z_c is the critical compressibility factor [25], and represent an additional dependence on Z_c which usuful for mixing models.

Complete definitions for a, b, α and δ_1 as well as their fitting parameters can be found in work of Cismondi and Mollerup [16].

2.2. Mixing rules

In order to extend the validity of the real fluid EoS to an arbitrary number of components, a mixture model is needed. A mixture can be considered as a unique pure hypothetical fluid whose parameters required by the EoS are calculated from conventional molar fraction based mixing rules [25] containing the individual species characteristics:

$$a\alpha = \sum_{i=1}^{ns}\sum_{j=1}^{ns} X_i X_j a_{ij}\alpha_{ij} \quad b = \sum_{i=1}^{ns} X_i b_i \qquad (2)$$

$$\delta_1 = \sum_{i=1}^{ns} X_i \delta_{1,i} \qquad (3)$$

where subscript i refers to the $i-$th species and X is the molar fraction. The off-diagonal terms $a_{ij}\alpha_{ij}$, representing binary interactions, are obtained by means of combination rules based on pseudo-critical parameters [26], and neglecting interaction parameters.

2.3. Thermodynamical properties of mixtures

Once the mixture is characterized by EoS parameters ($a\alpha$,b,δ_1), every thermodynamic relation can be expressed in terms of a reference ideal low-pressure property, denoted by subscript 0, and a real gas departure function [26] derived from the real gas EoS. Generally, such properties are not independent of each other so that an evaluation order has to be chosen. One common choice is to start from internal energy [27]:

$$e(T,\rho) = e_0(T) + \int_{\rho_0}^{\rho}\Big[\frac{p}{\rho^2} - \frac{T}{\rho^2}\Big(\frac{\partial p}{\partial T}\Big)_{\rho_i}\Big]d\rho \qquad (4)$$

The above expression of the mass based internal energy allows for the derivation of the single species internal energy e_i by differentiating with respect to the partial density [28]:

$$e_i = \Big(\frac{\partial \rho e}{\partial \rho_i}\Big)_{T,\rho_{j\neq i}}. \qquad (5)$$

The enthalpy of the species i is obtained from basic thermodynamics relations for a mixture of general gases.

$$h_i = e_i - \Big(\sum_{j=1}^{ns} Y_j e_j - e(T,\rho) - \frac{p}{\rho}\Big)\frac{\Big(\frac{\partial p}{\partial \rho_i}\Big)_{T,\rho_{j\neq i}}}{\Big(\frac{\partial p}{\partial \rho}\Big)_{T,Y_i}} \qquad (6)$$

where Y is the mass fraction and where the specific enthalpy of the mixture can be obtained simply by the definition $h = \sum_{i=1}^{ns} Y_i h_i$.

The specific heat capacity at constant volume is evaluated differentiating the internal energy definition with respect to the temperature.

$$c_v = \Big(\frac{\partial e}{\partial T}\Big)_{Y_i,\rho} \qquad (7)$$

Once c_v is determined other properties such as specific heat capacity at constant pressure and speed of sound can be evaluated using fundamental thermodynamical relationship [28]:

$$c_p = c_v + \frac{T}{\rho^2}\frac{\Big(\frac{\partial p}{\partial T}\Big)^2_{\rho_i}}{\Big(\frac{\partial p}{\partial \rho}\Big)_{Y_i,T}} \qquad (8)$$

The expressions reported above are independent from the EoS, only the explicit form of the thermodynamic derivatives depend on the particular form of the EoS used. In the present case of RK-PR EoS they assume the form derived by Kim et al. [17].

2.4. Supercritical Flamelet equations

The local flame structures of a turbulent flame can be effectively described by the laminar flamelet equations which represent an unsteady competition between the chemical kinetics and molecular diffusion processes enhanced by turbulent mixing. The key parameter of the flamelet equation is the scalar dissipation rate χ which governs the non-equilibrium effects, where the steady-state solution for $\chi = 0$ effectively represents thermodynamic equilibrium. With the unitary Lewis-number assumption the classical form of the flamelet equations reads [29]:

$$\frac{\partial Y_i}{\partial t} = \frac{1}{2}\chi\frac{\partial^2 Y_i}{\partial z^2} + \frac{\dot{\omega}_i}{\rho} \qquad (9)$$

$$\frac{\partial T}{\partial t} = \frac{1}{2}\chi\Big[\frac{\partial^2 T}{\partial z^2} + \frac{1}{c_p}\frac{\partial c_p}{\partial z}\frac{\partial T}{\partial z}\Big] + \frac{\dot{\omega}_T}{c_p\rho} \qquad (10)$$

where z is the mixture fraction and $\dot{\omega}_i$ the mass production rate. The mixture c_p experiences abrupt changes when the mixture undergoes a transcritical transition causing discretization issues of its numerical derivative with respect to z. Therefore an equivalent energy equation can be used instead of Eq. (10), substituting the derivatives of temperature and c_p with the second derivative of enthalpy with respect to the mixture fraction [30]:

$$\frac{\partial T}{\partial t} = \frac{1}{2}\chi\frac{1}{c_p}\Big[\frac{\partial^2 h}{\partial z^2} + \sum_{k=1}^{ns} h_k\frac{\partial^2 Y_k}{\partial z^2}\Big] + \frac{\dot{\omega}_T}{c_p\rho} \qquad (11)$$

Equations (9) and (11) define the flamelet equations system, whose solution is the flame structure. The time dependent flame structure is calculated by means of the Rflamelet in-house code, which uses a stiff solver for ordinary differential equations (DVODE) and the Chemkin-II package [31] together with a real gas correction library which implements the departure functions for real thermodynamical properties for a general cubic equation of state.

2.5. Real Gas reaction rates

Detailed reaction mechanisms for combustion, such as those in Chemkin format, usually provide Arrhenius rate constants k_f for forward steps only. The reverse rate constant k_r of the j-th reaction is then obtained using

equilibrium criteria [31] and the equilibrium constant K_c so that $K_{r_j} = k_{f_j}/k_{c_j}$. This expression holds for both ideal and real gases, but if the perfect gas EoS is considered, K_c is a function of the temperature only while in the general case it carries an additional dependence on pressure. According to this consideration a correction for real gases is needed such as:

$$K_{c_j}^{real} = K_{c_j}^{ideal} K_{c_j}^{corr} \tag{12}$$

where $K_{c_j}^{corr}$ is the correction factor that takes into account fugacity and compressibility effects [32]. These effects are usually neglected in calculations [19], however, to the best of our knowledge, a detailed analysis is still missing in the current literature.

3. Results and Discussion

Before analyzing the unsteady flame structure of the high pressure methane-LOx combustion, a validation of the present model is briefly reported. The thermodynamical properties for both the fuel and the oxidizer are compared against NIST data obtained with the Refprop software[33]. The chemical mechanism chosen, Ramec [34], includes 38-species and 190-reaction steps, has been employed here to cover high pressure and low temperature conditions. This mechanism has been developed starting from the GRI-Mech 1.2 adding 12 reactions and 6 species. These additional reactions and species have been identified to play an important role in the oxidation of methane at high-pressures. In particular they correctly reproduce, with respect to experimental data [15], the high pressure ignition delay times, consistently smaller than at lower pressure.

3.1. Thermodynamics properties validation

In the proximity of the critical point, thermodynamic and transport properties exhibit anomalies in their behavior, usually referred as near-critical enhancement. In figures 1 thermophysical properties, important for flamelet solutions such as density and specific heat at constant pressure, are compared with those of NIST for pure oxygen at various pressures and within a temperature range of interest. The interface between dense liquid and light gas is represented by steep gradients, which are captured accurately by the Rflamelet code even if smooth curves (due to the cubic EoS) are present instead of a sharp interface. It is important to note that the specific heat at constant pressure deviates the Refprop results close to the transcritical regime for both methane and oxygen. This is not a major drawback since, in the present study, we are interested in high

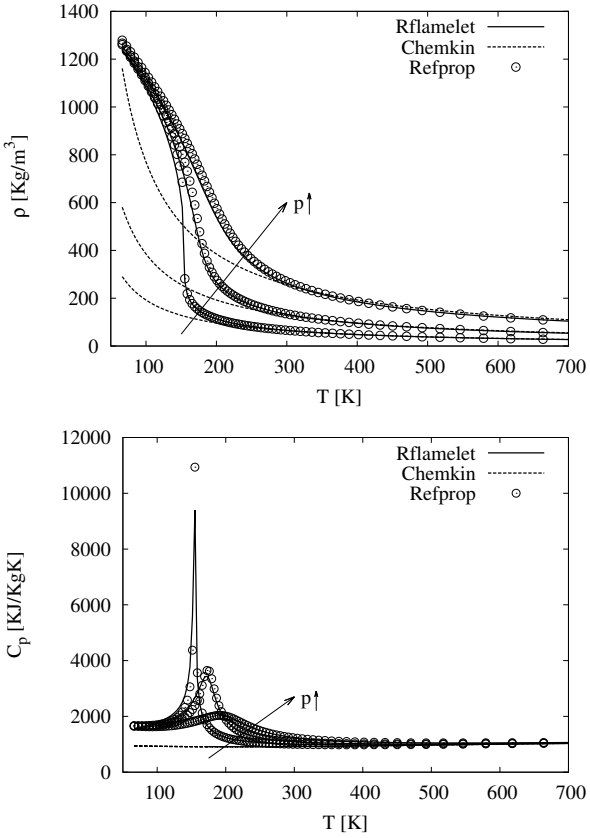

Figure 1: Density of pure oxygen as a function of temperature at three different pressures, respectively 5MPa, 10MPa and 20MPa.

pressures which are well above the critical ones of the propellants considered.

3.2. Autoignition test case definition

A pressure of 6MPa is chosen as representative of a LOx-Methane LRE chamber pressure. This pressure value is particularly challenging from a numerical point of view because it is near the critical region for the pure oxygen side ($T_{cr} = 154.6K$, $p_{cr} = 5.043MPa$). This means that a high resolution grid in the mixture fraction space is required at the lean side. A non-uniform 128 point grid is used in this case, in order to correctly capture the near critical enhancement of the thermophysical properties. The present case is characterized by a constant scalar dissipation rate ($\chi = 10s^{-1}$), a cold oxidizer side ($T_{ox} = 120K$) and an hot fuel side ($T_f = 1400K$), which allows autoignition in the rich zone.

3.3. Unsteady Flame Structure

Starting from the mixing lines as initial condition, temperature at first exhibits a small increase in the rich region, in the neighborhood of the most reactive mixture fraction ($z_{MR} \simeq 0.7$) while some pre-ignition species (CH_3, HO_2 , H_2O_2) increase gradually, before autoignition occurs. This time is usually referred to as induction time [35]. After such induction time, the species related to highly exothermic processes, such as the final products of combustion (e.g. CO in Fig. 2), as well as temperature, increase abruptly, approaching the final steady flamelet profile, while pre-ignition species are rapidly consumed. At this stage autoignition occurs and an autoignition time can thus be defined.

Autoignition time, in the high-pressures regime, is significantly shorter than at lower pressures due to pressure influence on the chemical reactions paths involving the species CH_3O_2, not included in the original GRI-Mech 1.2 [34]. In this case autoignition can be considered to happen at about 1.2ms, regardless of the kind of autoignition marker used. This usually indicates that the mixture does not experience multiple ignition events, such as those observed with higher hydrocarbons.

After autoignition occurs, a typical transient evolution usually exhibits a lean and a rich premixed reaction front propagating in opposite directions in mixture fraction space [35]. In this particular case the rich reaction front is almost invisible because autoignition occurs at very rich mixtures close to the fuel boundary ($z = 1$). The lean front soon approaches the stoichiometric zone and is then extinguished in the high density lean region, while the trailing temperature profile is the final steady state flame structure. The propagation speed of the premixed fronts strongly depends on the stoichiometric value of the scalar dissipation rate as well as on its functional profile in the $z-$space. This effect, however, is not investigated here.

3.4. Constant pressure specific heat behavior

The profile of $C_p(z)$ at $t = 0$s shown in Fig.(3) in $z-$space, displays a critical enhancement due to the combined effect of composition, being close to that of pure oxygen ($z \simeq 1$), and temperature being close to the critical temperature of oxygen ($T(z) \simeq T_{O_2}^{critical} =$ 154.6K). At later times, the lean premixed front, traveling towards leaner mixtures, begins to interact with the localized $C_p(z)$ enhancement. Because, by its own definition, the latter occurs where the temperature profile approaches the critical value at the local composition in $z-$space, the peak is gradually shifted towards the lean side as the local temperature is increasing due to the approaching lean front. The $C_p(z)$ enhancement acts as a barrier for the propagation of the lean front as it essentially acts as a heat sink for the energy equation. This substantially slows the lean front thus delaying the attainment of steady state flame structure.

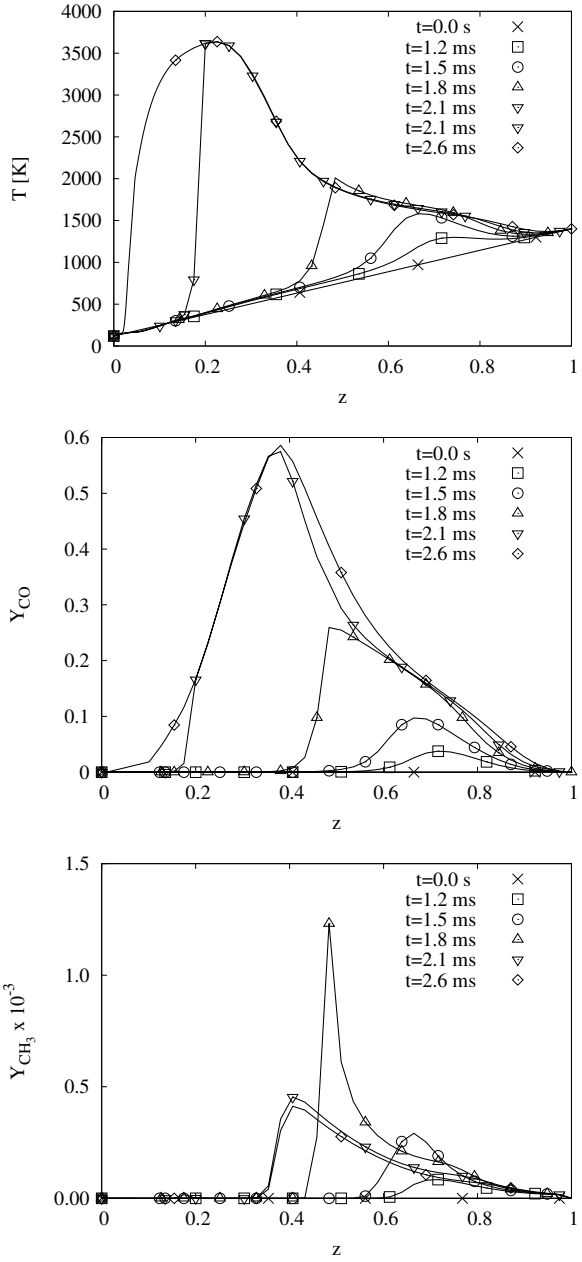

Figure 2: Unsteady Flame Structure of the LOx-Methane mixture at 6MPa, at different time steps in terms of temperature (top), Y_{CO} (middle) and Y_{CH_3} (bottom).

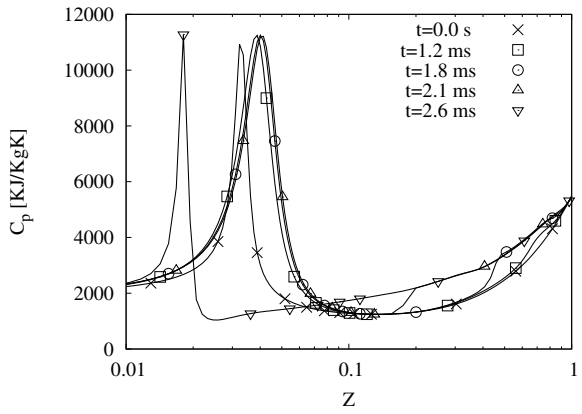

Figure 3: Unsteady time evolution of a representative thermophysical property: constant pressure specific heat at 6MPa

4. Conclusions

The direct flamelet equation approach in mixture fraction space has been used to investigate the unsteady flame structure of supercritical LOx-Methane combustion. Real gas effects have been taken into account by means of a general form cubic equation of state. High-pressure conditions of 6MPa have been chosen as a representative of a methane/liquid-oxygen rocket engine operating conditions. An autoignition test case has been chosen in order to investigate the interaction of the real fluid effects with the ignition processes without introducing any external energy source. Complete ignition time of the flamelet has been shown to be effectively influenced by real fluid effects. The role of constant pressure specific heat in the evolution of the flame structure has been analyzed, showing the traveling of C_p peak in the mixture fraction space and its acting like a barrier for the reaction front in the lean side. The in-house developed Rflamelet code has been shown to be able to constitute the very first building block, as an unsteady general fluid flamelet solver, of a conditional moment closure for supercritical turbulent combustion.

References

[1] G. Sutton, History of Liquid Propellant Rocket Engine, AIAA, Reston, VA, 2005.

[2] D. Preclik, G. Hagemann, O. Knab, L. Brummer, C. Mäding, D. Wiedmann (2005).

[3] A. Urbano, F. Nasuti, Journal of Propulsion and Power 30 (2014) 153–163.

[4] N. Zong, V. Yang, Proceedings of the Combustion Institute 31 (2007) 2309–2317.

[5] V. Yang, N. Zong, International Journal of Computational Fluid Dynamics 21 (2007) 217–230.

[6] T. Kim, Y. Kim, S.-K. Kim, The Journal of Supercritical Fluids 58 (2011) 254–262.

[7] S. Candel, T. Schmitt, M. Boileau, Y. Méry, Proceedings of the Combustion Institute 33 (2011) 1383–1390.

[8] T. Kim, Y. Kim, S.-K. Kim, The Journal of Supercritical Fluids 81 (2013) 164–174.

[9] S. Candel, M. Juniper, G. Singla, P. Scouflaire, C. Rolon, Combustion Science and Technology 178 (2006) 161–192.

[10] P. Scouflaire, J.-C. Rolon, S. Candel, M. Juniper, a. Tripathi, Proceedings of the Combustion Institute 28 (2000) 1103–1109.

[11] G. Singla, P. Scouflaire, C. Rolon, S. Candel, Proceedings of the Combustion Institute 30 (2005) 2921–2928.

[12] G. Singla, P. Scouflaire, C. Rolon, S. Candel, Combustion and Flame 144 (2006) 151–169.

[13] M. Habiballah, M. Orain, F. Grisch, L. Vingert, P. Gicquel, Combustion Science and Technology 178 (2006) 101–128.

[14] V. Yang, Proceedings of the Combustion Institute 28 (2000) 925–942.

[15] D. F. Davidson, R. K. Hanson, E. L. Petersen, M. Ro, C. T. Bowman, International Journal of Chemical Kinetics (1996) 799–806.

[16] M. Cismondi, J. r. Mollerup, Fluid Phase Equilibria 232 (2005) 74–89.

[17] S.-K. Kim, H.-S. Choi, Y. Kim, Combustion and Flame 159 (2012) 1351–1365.

[18] L. Pons, N. Darabiha, S. Candel, T. Schmitt, B. Cuenot, Comptes Rendus Mécanique 337 (2009) 517–527.

[19] V. Yang, N. Darabiha, G. Ribert, L. Pons, N. Zong, S. Candel, Combustion and Flame 154 (2008) 319–330.

[20] S. Candel, L. Pons, N. Darabiha, V. Yang, G. Ribert, Combustion Theory and Modelling 13 (2009) 57–81.

[21] G. Lacaze, J. C. Oefelein, Combustion and Flame 159 (2012) 2087–2103.

[22] X. Wang, H. Huo, V. Yang, AIAA SciTech, 51st Aerospace Sciences Meeting (2013).

[23] H. Huo, X. Wang, V. Yang, Combustion and Flame 161 (2014) 3040–3050.

[24] X. Wang, H. Huo, V. Yang (2014) 1–14.

[25] R. Reid, J. Prausnitz, B. Poling, The properties of Gases and Liquids, McGraw-Hill, New York, NY, 2001.

[26] R. S. Miller, J. Bellan, AIChE Journal 43 (1997) 4–9.

[27] H. Meng, V. Yang, Journal of Computational Physics 189 (2003) 277–304.

[28] B. Younglove, Journal of Chemical Refence Data 11 (1982).

[29] N. Peters, The properties of Gases and Liquids, Cambridge University Press, Cambridge, UK, 2000.

[30] T. Kim, Y. Kim, S.-K. Kim, International Journal of Hydrogen Energy 36 (2011) 6303–6316.

[31] R. Kee, F. Rupley, J. Miller, Chemkin II: A FORTRAN package for analysys of gas phase chemical kinetics, Sandia National Laboratories, 1993.

[32] W. Tang, K. Brezinsky, International Journal of Chemical Kinetics 38 (2006) 75–97.

[33] Refprop, http://webbook.nist.gov/chemistry/fluid, National Institute of Standards and Technology Webbook, 2014.

[34] E. L. Petersen, D. F. Davidson, R. K. Hanson 290 (1999) 272–290.

[35] E. Mastorakos, Progress in Energy and Combustion Science 35 (2009) 57–97.